PHOTONICS Research

Scalable and highly efficient approach for an on-chip single-photon source

Xingyu Chen, Rongbin Su,* Jin Liu, Juntao Li, and Xue-Hua Wang

State Key Laboratory of Optoelectronic Materials and Technologies, School of Physics, Sun Yat-sen University, Guangzhou 510000, China
*Corresponding author: surongbin@mail.sysu.edu.cn

Received 26 April 2022; revised 19 June 2022; accepted 28 June 2022; posted 30 June 2022 (Doc. ID 462318); published 15 August 2022

Integrated photonic circuits with quantum dots provide a promising route for scalable quantum chips with highly efficient photonic sources. However, unpolarized emission photons in general sacrifice half efficiency when coupling to the waveguide fundamental mode by a cross polarization technique for suppressing the excitation laser, while suspended waveguide photonics sources without polarization filters have poor scalability due to their mechanical fragility. Here, we propose a strategy for overcoming the challenge by coupling an elliptical Bragg resonator with waveguides on a solid-state base, featuring near-unity polarization efficiency and enabling on-chip pulsed resonant excitation without any polarization filters. We theoretically demonstrate that the proposed devices have outstanding performance of a single-photon source with 80% coupling efficiency into on-chip planar waveguides and an ultra-small extinction ratio of 10^{-11}, as well as robustness against quantum dot position deviation. Our design provides a promising method for scalable quantum chips with a filter-free high-efficiency single-photon source.

https://doi.org/10.1364/PRJ.462318

1. INTRODUCTION

Photonic quantum information processing has given birth to a wide array of emerging quantum technologies, such as quantum computing [1,2], quantum communications [3,4], quantum repeaters [5,6], and ultimately a full-fledged quantum Internet [7,8]. Implementing these techniques requires the bright and deterministic emission of background-free single photons into a given quantum state. Ideally, the single photons emitted at different time should be indistinguishable, including polarization, spatial mode, and transform-limited spectrotemporal profile, for high-visibility Hong–Ou–Mandel type quantum interference [9]. For on-chip quantum photonic circuits, single photons should be efficiently coupled to a waveguide for processing photons with high-fidelity operators on-chip [10].

So far, self-assembled semiconductor quantum dots (QDs), showing high quantum efficiency in solid-state quantum emitters, have become one of the most attractive candidates to serve as ideal single-photon emitters [11]. By eliminating dephasing and time jitter, pulsed resonant excitation on single QDs has achieved near-ideal single photons. Well-designed nano structures have shown the ability to improve the collection efficiency of emitted single photons and engineer their quantum properties by precisely controlling the environment of the emitter [12–14]. By combining resonant excitation with Purcell-enhanced microcavities [15–17], the generated near-ideal single-photon and entangled-photon pair sources have been efficiently extracted out of bulk.

In general, a cross-polarized excitation–collection scheme [18,19] is preferred for implementing pulsed resonant excitation of a QD. But this method inherently limits the collection efficiency of the generated single photons to ≤50%. Recently, to break through this limitation, polarized microcavities have been used to control the radiation characteristics of QDs [17,20], with an efficiency up to 60% in experiment [17,20]. But this efficiency is still short of the minimal efficiency threshold of 67%, which is needed for photon-loss-tolerant encoding in cluster-state models of optical quantum computing [21]. Furthermore, the excitation and collection of single photons in polarized microcavities still use the same channel in free space, and still need a sophisticated post-filtration process, therefore limiting the scalability of photonic quantum information applications such as boson sampling [22,23].

Integrating QDs within on-chip waveguide circuits is a promising approach to achieve high coupling efficiency and source scalability without a filter [24–26]. Here the coupling efficiency is defined as the number of single photons extracted from bulk and coupled into the fundamental mode of the on-chip waveguide per pumping pulse. The excitation and collection can be set orthogonally in planar nanophotonic waveguides, which can suppress the excitation laser efficiently even without any optical filter [27]. Suspended waveguides such as a photonic crystal waveguide [28] or nanobeam waveguide [29,30] are highly efficient platforms for integrated quantum circuits with single photons based on QDs, but have poor

scalability due to their mechanical fragility. Moreover, for unpolarized quantum state of QDs, such as a charged exciton, nanobeam waveguides suffer from considerable loss due to other polarized single-photon emission, which is orthogonal to waveguide TE modes. Nanobeam waveguides rarely suppress the unwanted polarized single-photon emission; even in a photonic crystal waveguide, the suppression is not enough, retaining a Purcell factor >0.2. Furthermore, QDs are always close to the etched sides of planar nanophotonic waveguides. For example, to achieve coupling efficiency of 60% for unpolarized QDs, the width of a bare waveguide is 0.25λ [31]. That means that the QD is just 120 nm away from the etched waveguide edge. In this situation, the charge fluctuations from the etching surfaces close to QDs significantly reduce photon indistinguishability [32,33], and need to be suppressed by more complicated methods, e.g., surface passivation [34] or gate control [28,35]. Hence, controlling the polarization of single photons from a QD to match the waveguide mode and implement highly efficient, robust coupling remains a formidable challenge.

Here, we propose an elliptical Bragg resonator with coupling waveguides on a solid-state base to achieve near-unity polarization efficiency and coupling efficiency of 80% without post-filter operation. In addition, the proposed structures are placed on SiO_2 buffer layers that can support large-scale implementation. The QD sits at the center about 400 nm away from the etching surface, avoiding the deterioration of QD fluorescence.

2. THEORETICAL SCHEME

To get an on-demand and truly scalable high-performance source of indistinguishable single photons, we propose an elliptical Bragg resonator with coupling waveguides on the SiO_2 solid-state substrate [Fig. 1(a)]. This structure can achieve a background-free excitation signal without sacrificing system efficiency, while coupling the generated single photon into the planar waveguide fundamental mode with high efficiency.

As shown in Fig. 1(a), a polarized microcavity called an elliptical Bragg resonator supports two-fold non-degenerate cavity modes [17], i.e., horizontal polarization (H-Pol) and vertical polarization (V-Pol) modes. The pulsed resonance excitation laser with H-Pol excites the solid-state quantum emitters (e.g., QDs) embedded in the central elliptical disk of the resonator. This excitation light, which cannot be coupled to the waveguide fundamental mode due to the space pattern mismatch and polarization orthogonality of their mode fields, will be suppressed efficiently in the on-chip waveguide. The elliptical Bragg resonator can also selectively enhance or suppress the different polarization fluorescence of the emitter in the middle of the resonator. Hence, only the excited emitter (e.g., QDs) matching the V-Pol resonating mode can emit V-Pol single-photon streams efficiently due to polarization-dependent Purcell enhancement [17]. These V-Pol single photons can be further coupled into the fundamental mode of the two waveguides with high coupling efficiency [see Fig. 1(b)]. There are some advantages of this scheme: (1) it can overcome the 50% efficiency limit of conventional resonance excitation and enhance the on-chip coupling efficiency of single photons; (2) the excitation light and single photons are distributed in different channels, which is essentially suitable for experimental implementation of the filter-free pulsed resonant excitation scheme; (3) it separates coherent single photons into two symmetric on-chip waveguides, functioning as an integration beam splitter, an essential component in photon-based quantum computing [23].

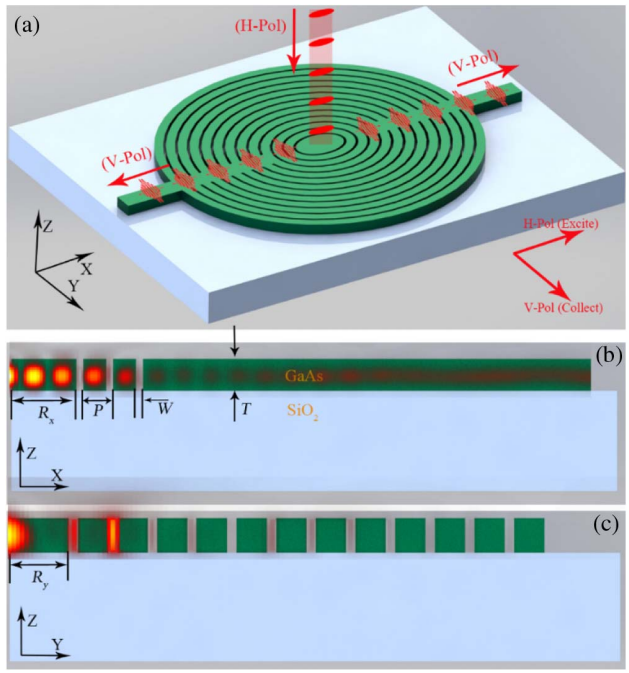

Fig. 1. Schematic diagram of elliptical Bragg resonator with coupling waveguides for generation of on-chip single photons. (a) The elliptical Bragg resonator with coupling waveguides consists of an elliptical disk with quantum emitter in the center, fully etched elliptical Bragg gratings, and coupling waveguides on the long axis of the elliptical disk. The substrate of the structure is a thick low-refractive-index layer (e.g., silica). (b) Cross section with superimposed cavity mode electric field of the elliptical Bragg resonator with coupling waveguides in x direction. R_x is the radius of the central disk on x axis (long axis). P, W, period and grating spacing of the Bragg grating, respectively; T, thickness of the structure. (c) Cross section with superimposed cavity mode electric field of the elliptical Bragg resonator with coupling waveguide in y direction. R_y is the radius of the central disk on the y axis (short axis).

The on-chip coupling efficiency η of a single photon is quantified through the polarization efficiency η_p and the β-factor:

$$\eta = \eta_p \times \beta, \tag{1}$$

where the polarization efficiency η_p is defined as the ratio of the V-Pol photons to the total photons emitted by the quantum emitter, and the β-factor is defined as the probability of the V-Pol photons being collected into the fundamental mode of the two symmetric waveguides. Therefore, to achieve high on-chip coupling efficiency η, elliptical Bragg resonators should be designed to achieve high polarization efficiency η_p, and the coupling waveguide should be designed to efficiently couple the V-Pol photons from elliptical Bragg resonators (high β-factor). Furthermore, it is necessary to implement a moderate Purcell

factor at the same wavelength as the high coupling efficiency for two main reasons: (1) moderate Purcell enhancement can effectively accelerate the radiation rate of QDs to enhance the indistinguishability of single photons in a cavity [19]; (2) the Purcell effect can reduce the radiation lifetime of QDs to improve the absolute brightness.

3. ELLIPTICAL BRAGG RESONATORS

Circular Bragg resonators, tightly confining the light in a sub-λ transverse plane, have been used on solid-state quantum emitters for enhancing their out-of-plane collection efficiencies [36,37]. To further improve collection efficiency, a low-refractive-index SiO_2 layer with tightly controlled thickness and a gold mirror were added at the bottom of the resonator to suppress downwards photon leakage [38–40]. Recently, elliptical Bragg resonators were also proposed to break the original polarization symmetry of QD emission, overcoming the efficiency limit of resonance fluorescence [17]. Unlike most of these circular/elliptical Bragg resonators with second-order Bragg gratings for improving the out-of-chip collection efficiency, we design an elliptical Bragg resonator with a first-order Bragg grating for coupling single photons to the in-plane waveguide. Here, first- and second-order Bragg gratings are defined as $P = \frac{1}{2}\lambda_0/n_{\text{eff}}$ and $P = \lambda_0/n_{\text{eff}}$, respectively, where P is the period of the Bragg grating, λ_0 is the free space wavelength of QD, and n_{eff} is the effective refractive index of the Bragg grating (see Appendix B for more details).

We design a GaAs-based elliptical Bragg resonator with the center disk embedding an InAs QD, surrounded by a first-order Bragg grating on the SiO_2 substrate. Considering the spectral random distribution of QDs and fabrication tolerance, the thickness of the GaAs (T), period (P), and grating spacing (W) of the Bragg grating are set to be 160 nm, 170 nm, and 40 nm, respectively.

The elliptical Bragg resonator supports two-fold orthogonal cavity modes, one in H-Pol and the other in V-Pol. These two modes are very sensitive to the size and ellipticity of the center disk. Here, the degree of ellipticity ρ can be defined as

$$\rho = \frac{R_x - R_y}{R_x}, \tag{2}$$

where R_x (R_y) is the long axis (short axis) of the center disk, and R_x is set to 398 nm.

When coupling a single-electron charged QD to this elliptical Bragg resonator, the inherent orthogonal polarization symmetry of QD emission will be broken. As a result, its spontaneous emission rate will be redistributed into the V-Pol and H-Pol. As shown in Fig. 2, a 1% ellipticity results in a 2.3 nm split between the Purcell factor peaks of the cavity H mode and cavity V mode [see Fig. 2(b)]. The splitting width will increase to 14 nm when increasing the ellipticity to 5% [see Fig. 2(c)]. The Purcell factor peak of the cavity H mode will blueshift out of our working wavelength window when the degree of ellipticity ρ becomes larger [Fig. 2(d)].

Figure 2(e) shows the polarization efficiency of the elliptical Bragg resonator with different ellipticities. Here, the polarization efficiency η_p can be quantified according to the Purcell factor of the cavity V mode [F_p(V)] and H mode [F_p(H)]:

$$\eta_p = \frac{F_p(\text{V})}{F_p(\text{V}) + F_p(\text{H})}. \tag{3}$$

For the circular Bragg resonator [$\rho = 0$ in Fig. 2(a)], the H and V modes of the resonators equally enhance the QD emission, resulting in polarization efficiency of $\eta_p = 50\%$.

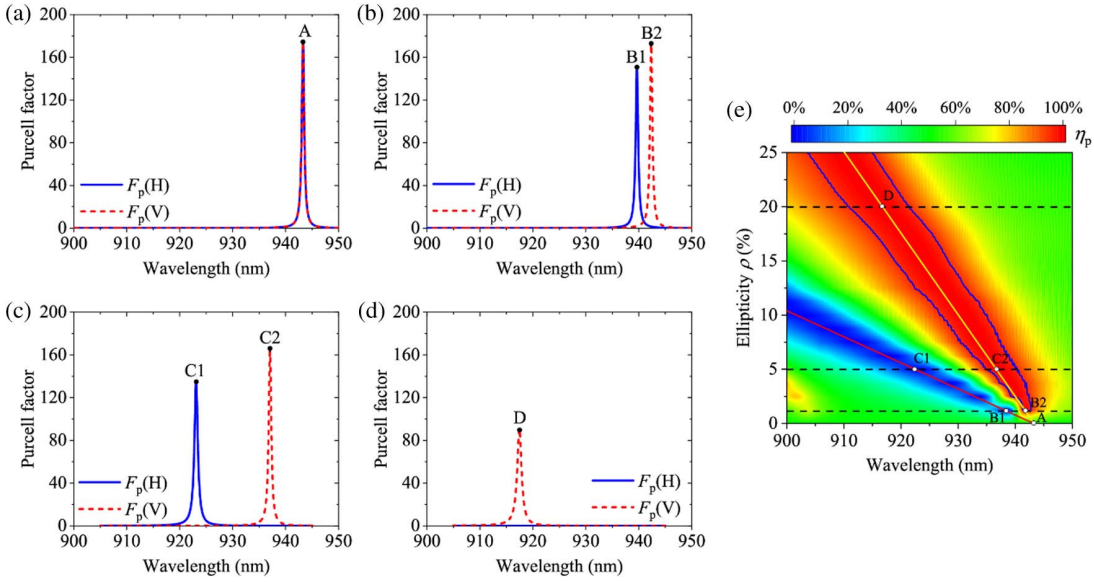

Fig. 2. Purcell factor distribution and polarization efficiency of the resonator with different ellipticities. Purcell factor as a function of wavelength with different ellipticities of (a) $\rho = 0$, (b) $\rho = 1\%$, (c) $\rho = 5\%$, and (d) $\rho = 20\%$. Points A, B1, B2, C1, C2, and D are the Purcell factor peaks of the resonators with different ellipticities, also shown in (e). (e) Polarization efficiency of preparing V-Pol single photons for a QD coupling to the resonator with different ellipticities. Yellow and red lines correspond to cavity peaks, i.e., Purcell factor peaks of V and H modes, respectively. The blue curve represents 95% polarization efficiency contour line. In simulations, the radius of the central disk on x axis (long axis) is selected as $R_x = 398$ nm.

This 50% limitation of polarization efficiency can be broken by using the elliptical Bragg resonator to move the cavity H mode (red line) away from the cavity V mode (yellow line), as Fig. 2(e) shows. An ellipticity of 1% (bottom black dashed line) is enough for inducing cavity mode splitting and then preparing the polarized single photons with near-unity polarization efficiency. With the increase in ellipticity, the bandwidth of achieving high polarization single-photon efficiency increases. For example, an ellipticity of 20% can achieve 95% polarization efficiency with a bandwidth of 11 nm (top black dashed line), which can cover the spectral random distribution of QD emission. This near-unity polarization efficiency originates from strong suppression of the cavity H mode as low as $F_p(\mathrm{H}) \leq 0.05$ in a two-dimensional polarized cavity. The suppression is close to an order of magnitude stronger than that in a planar waveguide or photonic crystal waveguide.

4. COMBINATION ELLIPTICAL BRAGG RESONATORS WITH COUPLING WAVEGUIDES

After designing the elliptical Bragg resonator with near-unity polarization efficiency, we add the coupling waveguides to achieve both a high β-factor and high Purcell factor of the cavity V mode at the same wavelength.

As the waveguide approaches the central disk, more photons can leak out to the waveguide, achieving a high β-factor. Meanwhile, the cavity mode will be destroyed, and the Purcell factor will decrease significantly due to the breaking of the reflectivity of the Bragg reflector. Therefore, we connect the coupling waveguides to the third ring of the elliptical Bragg grating in our design.

As shown in Figs. 3(a) and 3(b), the β-factor and Purcell factor as functions of wavelength are dependent on the width of the waveguide W_d and the ellipticity ρ. We note that the regions with high β-factors (>0.8) do not always overlap with those of high Purcell factors (>5). To obtain a good combination of the β-factor, Purcell factor, and operation bandwidth, we choose the following set of design parameters: $W_d = 485$ nm and $\rho = 20\%$. Under these parameters and within a 9 nm bandwidth from 914 nm to 923 nm, the on-chip coupling efficiency and Purcell factor of the cavity V mode can be larger than 70% and 5, respectively [Fig. 3(c)]. In spite of the decrease in Purcell factor of the cavity V mode due to the presence of waveguides, we can still get near-unity polarization efficiency because the strong suppression of the cavity H mode is maintained with $F_p(\mathrm{H}) \leq 0.05$. The maximal coupling efficiency can reach 80% with polarization efficiency >99% at 921 nm [see Figs. 3(c) and 3(d)]. A dip in coupling efficiency at a wavelength of 907 nm is caused mainly by the low β-factor [Fig. 3(d)].

5. RESULTS AND DISCUSSION

The single-photon performance and fabrication feasibility of the elliptical Bragg resonator with coupling waveguides will be discussed after setting the parameters of this device.

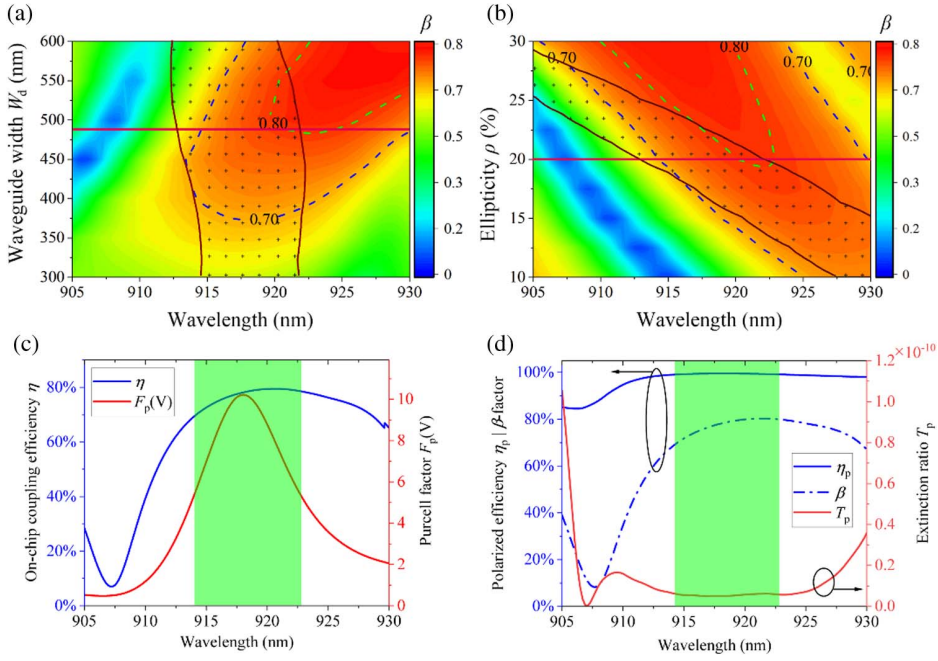

Fig. 3. Elliptical Bragg resonator with coupling waveguide for coupling polarized single photons. The β-factor as a function of wavelength for different (a) widths of the waveguide W_d and (b) values of ellipticity ρ. The area between the black solid lines corresponds to the V mode with Purcell factor >5. Blue and green dashed curves represent the 0.7 and 0.8 β-factor contour line, respectively. The ellipticity ρ and waveguide width W_d in (a) and (b) are set to 20% and 485 nm, respectively. The red lines in (a) and (b) correspond to $W_d = 485$ nm and $\rho = 20\%$, respectively. (c) On-chip coupling efficiency η (blue line) and Purcell factor of cavity V mode (red line) as a function of wavelength with the parameters of $W_d = 485$ nm and $\rho = 20\%$. (d) Polarization efficiency η_p (blue solid line), β-factor (blue dashed dotted line), and extinction ratio T_p (red line) as a function of wavelength with parameters of $W_d = 485$ nm and $\rho = 20\%$. The green shaded spectral region indicates spectral random distribution of QD emission from 914 nm to 923 nm.

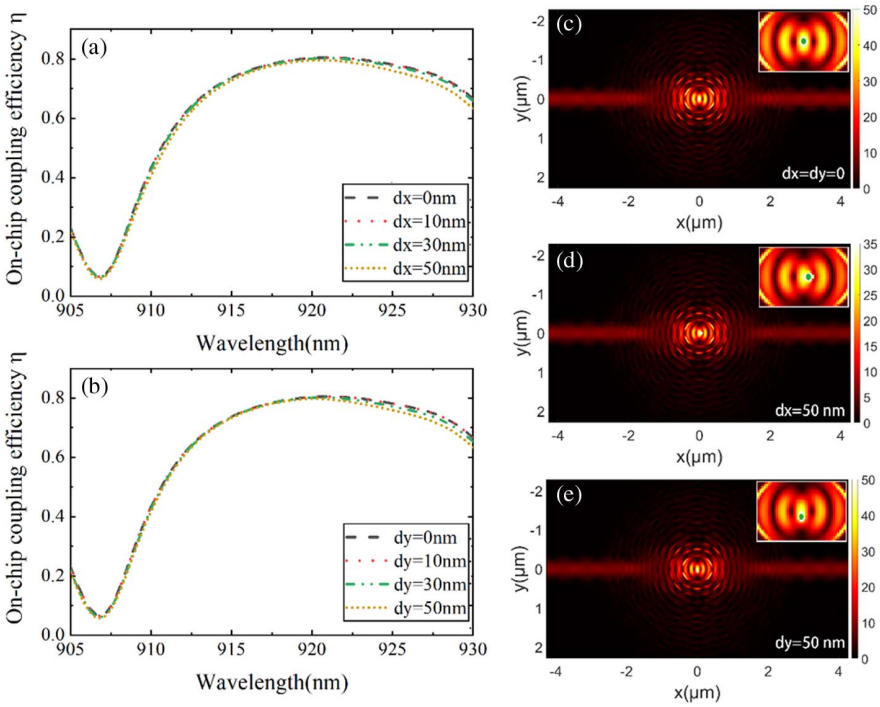

Fig. 4. Robustness of the elliptical Bragg resonator with coupling waveguide on SiO_2 substrate for on-chip single-photon source. On-chip coupling efficiency as a function of wavelength with QD position deviation in (a) x direction and (b) y direction from the resonator center. (c)–(e) Electric field distribution at a wavelength of 921 nm with different QD deviations. Insets show the position of QDs (green dots) and the electric field distribution of the center disk.

Extinction ratio. Sufficiently uncorrelated and weak noise are key prerequisites for quantum systems to solve computational problems, which are difficult for current digital computers to solve [41]. In a photonic quantum system, the noise is from the residual pump laser in the collection channel, and is more difficult to suppress in resonance excitation schemes. This problem can be overcome in our device by taking advantage of the waveguide mode and polarization selection. As shown in Fig. 3(d), our structure realizes a very high extinction ratio T_P of 10^{-11} without any filter for signal extraction, which can improve the single-photon performance [42]. Here, the extinction ratio T_P is defined as the transmittance of the pump laser into the single-photon collection channel, i.e., fundamental mode of the waveguide.

Fabrication feasibility. An ideal device for generation of single-photon sources should be easily implemented in experiments based on existing materials and technologies. Figures 4(a) and 4(b) show the coupling efficiency as a function of wavelength when the QD deviates from the resonator center. High and broadband coupling efficiency remains stable even if the QD is 50 nm away from the resonator center. That is because their electric field patterns are almost the same [Figs. 4(c)–4(e)]. Hence, we expect that this device can be deterministically fabricated by our QD positioning technique with 10 nm accuracy [43].

6. CONCLUSION

In conclusion, we have proposed an elliptical Bragg resonator with coupling waveguides for deterministic pulsed resonant excitation of single photons. Our simulations show that up to 80% of single photons can be coupled into the on-chip waveguide with a Purcell factor of seven. Furthermore, an extinction ratio of 10^{-11} enables filter-free resonant excitation, which is well suited for an efficient on-chip single-photon source. Our devices are compatible with the complementary metal–oxide–semiconductor process and can be experimentally implemented based on existing materials and technologies. With such an approach, the benefits of the scalable planar platform will be fully exploited in the ongoing pursuit of scaling up single-photon technology [44].

APPENDIX A: METHODS

The simulation is done by the finite-difference time-domain (FDTD) method from Lumerical Inc. F_p(V) and F_p(H) can be read from the Purcell factor of the dipole by placing a dipole in the center of the resonator, and the dipole orientation is vertical (horizontal) in the simulation. Six monitors are placed on the top, bottom, left, right, front, and back of the resonator. The total transmittance T_{all} of the dipole can be obtained by summing the absolute values of T in the six monitors. Monitor M_1 and mode monitor MM are placed on the waveguide interface to calculate the proportion of the fundamental mode power P_f. Then the β-factor can be calculated by $\beta = \frac{P_f}{P} \cdot \frac{T}{T_{\text{all}}}$, where P and T are the total power and total transmittance in monitor M_1, respectively. Similar to the β-factor, the extinction ratio T_P can be calculated as $T_P = \frac{P_f}{P} \cdot T$ by replacing the dipole with excitation light. The excitation light is a standard

H-Pol focused Gaussian beam with a beam waist of 2 μm at the center of the resonator.

APPENDIX B: FIRST-ORDER AND SECOND-ORDER BRAGG GRATINGS

For light propagating along a Bragg grating, the Bragg condition can be expressed as follows:

$$2Pn_{\text{eff}} = q\lambda, \tag{B1}$$

where P and n_{eff} are the period and effective refractive index of Bragg gratings, respectively, λ is the wavelength of light in free space, and q is the order of Bragg gratings. $q = 1$ gives the condition of a first-order grating, and $q = 2$ gives the condition of a second-order grating. The corresponding reciprocal lattice vector parallel to the interface is $G = 2\pi/P$.

The grating diffraction should satisfy the following relations:

$$k_{\parallel} = k - mG, \tag{B2}$$

and

$$k_{\parallel} \le nk_0 = n\frac{2\pi}{\lambda}, \tag{B3}$$

where $k_{\parallel}$ is the wave vector component parallel to the interface, m is an integer, indicating the diffraction order, and n is the surrounding refractive index.

For a first-order Bragg grating [Fig. 5(a)], $k_{\parallel} = k - G = -k$ and $k_{\parallel} = k$ can be supported, resulting in only parallel propagating lights of the interface. For a second-order Bragg grating [Fig. 5(b)], except for $k_{\parallel} = k - 2G = -k$ and $k_{\parallel} = k$, $k_{\parallel} = k - G = 0$ can also be supported, resulting in vertical propagating light for out-of-chip extraction.

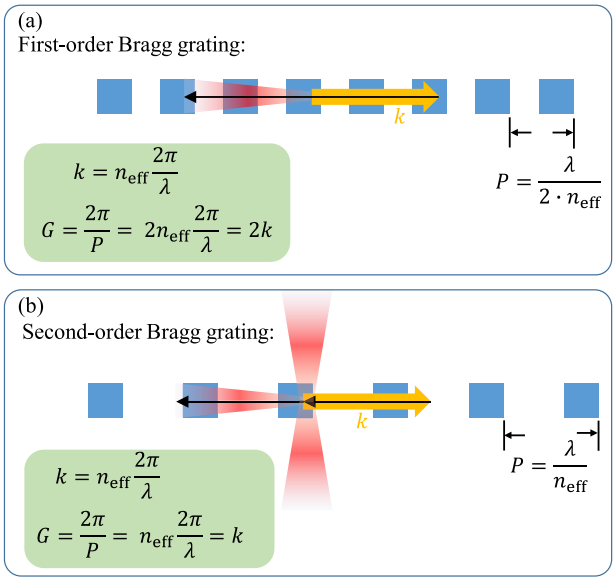

Fig. 5. Diffraction of (a) first-order and (b) second-order Bragg gratings. The yellow bold arrow indicates the initial light propagating wave vector. Black arrows superimposed on grating are the corresponding reciprocal lattice vector G.

Funding. National Key RD Program of China (2021YFA1400800); National Natural Science Foundation of China (11974436, 12104520); Key-Area Research and Development Program of Guangdong Province (2018B030329001); Guangdong Special Support Program (2019JC05X397); Basic and Applied Basic Research Foundation of Guangdong Province (2020B1515020019).

Disclosures. The authors declare no competing interests.

Data Availability. Data supporting the findings of this study are available within the paper and from the corresponding author upon reasonable request.

REFERENCES

1. P. Kok, W. J. Munro, K. Nemoto, T. C. Ralph, J. P. Dowling, and G. J. Milburn, "Linear optical quantum computing with photonic qubits," Rev. Mod. Phys. **79**, 135–174 (2007).
2. H.-S. Zhong, H. Wang, Y.-H. Deng, M.-C. Chen, L.-C. Peng, Y.-H. Luo, J. Qin, D. Wu, X. Ding, Y. Hu, P. Hu, X.-Y. Yang, W.-J. Zhang, H. Li, Y. Li, X. Jiang, L. Gan, G. Yang, L. You, Z. Wang, L. Li, N.-L. Liu, C.-Y. Lu, and J.-W. Pan, "Quantum computational advantage using photons," Science **370**, 1460–1463 (2020).
3. Z. Qi, Y. Li, Y. Huang, J. Feng, Y. Zheng, and X. Chen, "A 15-user quantum secure direct communication network," Light Sci. Appl. **10**, 183 (2021).
4. C. Schimpf, M. Reindl, D. Huber, B. Lehner, F. S. C. da Silva, S. Manna, M. Vyvlecka, P. Walther, and A. Rastelli, "Quantum cryptography with highly entangled photons from semiconductor quantum dots," Sci. Adv. **7**, eabe8905 (2021).
5. K. Azuma, K. Tamaki, and H.-K. Lo, "All-photonic quantum repeaters," Nat. Commun. **6**, 6787 (2015).
6. X. Liu, J. Hu, Z.-F. Li, X. Li, P.-Y. Li, P.-J. Liang, Z.-Q. Zhou, C.-F. Li, and G.-C. Guo, "Heralded entanglement distribution between two absorptive quantum memories," Nature **594**, 41–45 (2021).
7. S. Brito, A. Canabarro, R. Chaves, and D. Cavalcanti, "Statistical properties of the quantum internet," Phys. Rev. Lett. **124**, 210501 (2020).
8. S. Wehner, D. Elkouss, and R. Hanson, "Quantum internet: a vision for the road ahead," Science **362**, eaam9288 (2018).
9. H. Ollivier, S. E. Thomas, S. C. Wein, I. M. de Buy Wenniger, N. Coste, J. C. Loredo, N. Somaschi, A. Harouri, A. Lemaitre, I. Sagnes, L. Lanco, C. Simon, C. Anton, O. Krebs, and P. Senellart, "Hong-Ou-Mandel interference with imperfect single photon sources," Phys. Rev. Lett. **126**, 063602 (2021).
10. S. Hepp, M. Jetter, S. L. Portalupi, and P. Michler, "Semiconductor quantum dots for integrated quantum photonics," Adv. Quantum Technol. **2**, 1900020 (2019).
11. P. Senellart, G. Solomon, and A. White, "High-performance semiconductor quantum-dot single-photon sources," Nat. Nanotechnol. **12**, 1026–1039 (2017).
12. B. Chen, Y. Wei, T. Zhao, S. Liu, R. Su, B. Yao, Y. Yu, J. Liu, and X. Wang, "Bright solid-state sources for single photons with orbital angular momentum," Nat. Nanotechnol. **16**, 302–307 (2021).
13. Ł. Dusanowski, D. Köck, E. Shin, S.-H. Kwon, C. Schneider, and S. Höfling, "Purcell-enhanced and indistinguishable single-photon generation from quantum dots coupled to on-chip integrated ring resonators," Nano Lett. **20**, 6357–6363 (2020).
14. J. Liu, R. Su, Y. Wei, B. Yao, S. F. C. da Silva, Y. Yu, J. Iles-Smith, K. Srinivasan, A. Rastelli, J. Li, and X. Wang, "A solid-state source of strongly entangled photon pairs with high brightness and indistinguishability," Nat. Nanotechnol. **14**, 586–593 (2019).
15. H. Ollivier, I. Maillette de Buy Wenniger, S. Thomas, S. C. Wein, A. Harouri, G. Coppola, P. Hilaire, C. Millet, A. Lemaître, I. Sagnes, O. Krebs, L. Lanco, J. C. Loredo, C. Antón, N. Somaschi, and P. Senellart, "Reproducibility of high-performance quantum dot single-photon sources," ACS Photon. **7**, 1050–1059 (2020).

16. N. Tomm, A. Javadi, N. O. Antoniadis, D. Najer, M. C. Löbl, A. R. Korsch, R. Schott, S. R. Valentin, A. D. Wieck, A. Ludwig, and R. J. Warburton, "A bright and fast source of coherent single photons," Nat. Nanotechnol. **16**, 399–403 (2021).
17. H. Wang, Y.-M. He, T. H. Chung, H. Hu, Y. Yu, S. Chen, X. Ding, M. C. Chen, J. Qin, X. Yang, R.-Z. Liu, Z. C. Duan, J. P. Li, S. Gerhardt, K. Winkler, J. Jurkat, L.-J. Wang, N. Gregersen, Y.-H. Huo, Q. Dai, S. Yu, S. Höfling, C.-Y. Lu, and J.-W. Pan, "Towards optimal single-photon sources from polarized microcavities," Nat. Photonics **13**, 770–775 (2019).
18. A. V. Kuhlmann, J. Houel, D. Brunner, A. Ludwig, D. Reuter, A. D. Wieck, and R. J. Warburton, "A dark-field microscope for background-free detection of resonance fluorescence from single semiconductor quantum dots operating in a set-and-forget mode," Rev. Sci. Instrum. **84**, 073905 (2013).
19. F. Liu, A. J. Brash, J. O'Hara, L. M. P. P. Martins, C. L. Phillips, R. J. Coles, B. Royall, E. Clarke, C. Bentham, N. Prtljaga, I. E. Itskevich, L. R. Wilson, M. S. Skolnick, and A. M. Fox, "High Purcell factor generation of indistinguishable on-chip single photons," Nat. Nanotechnol. **13**, 835–840 (2018).
20. U. M. Gür, M. Mattes, S. Arslanagić, and N. Gregersen, "Elliptical micropillar cavity design for highly efficient polarized emission of single photons," Appl. Phys. Lett. **118**, 061101 (2021).
21. M. Varnava, D. E. Browne, and T. Rudolph, "How good must single photon sources and detectors be for efficient linear optical quantum computation?" Phys. Rev. Lett. **100**, 060502 (2008).
22. J. C. Loredo, M. A. Broome, P. Hilaire, O. Gazzano, I. Sagnes, A. Lemaitre, M. P. Almeida, P. Senellart, and A. G. White, "Boson sampling with single-photon Fock states from a bright solid-state source," Phys. Rev. Lett. **118**, 130503 (2017).
23. H. Wang, J. Qin, X. Ding, M.-C. Chen, S. Chen, X. You, Y.-M. He, X. Jiang, L. You, Z. Wang, C. Schneider, J. J. Renema, S. Höfling, C.-Y. Lu, and J.-W. Pan, "Boson sampling with 20 input photons and a 60-mode interferometer in a 10^{14}-dimensional Hilbert space," Phys. Rev. Lett. **123**, 250503 (2019).
24. M. Arcari, I. Söllner, A. Javadi, S. Lindskov Hansen, S. Mahmoodian, J. Liu, H. Thyrrestrup, E. H. Lee, J. D. Song, S. Stobbe, and P. Lodahl, "Near-unity coupling efficiency of a quantum emitter to a photonic crystal waveguide," Phys. Rev. Lett. **113**, 093603 (2014).
25. J. Q. Grim, A. S. Bracker, M. Zalalutdinov, S. G. Carter, A. C. Kozen, M. Kim, C. S. Kim, J. T. Mlack, M. Yakes, B. Lee, and D. Gammon, "Scalable in operando strain tuning in nanophotonic waveguides enabling three-quantum-dot superradiance," Nat. Mater. **18**, 963–969 (2019).
26. R. Uppu, H. T. Eriksen, H. Thyrrestrup, A. D. Uğurlu, Y. Wang, S. Scholz, A. D. Wieck, A. Ludwig, M. C. Löbl, R. J. Warburton, P. Lodahl, and L. Midolo, "On-chip deterministic operation of quantum dots in dual-mode waveguides for a plug-and-play single-photon source," Nat. Commun. **11**, 3782 (2020).
27. H. Thyrrestrup, G. Kiršanskė, H. Le Jeannic, T. Pregnolato, L. Zhai, L. Raahauge, L. Midolo, N. Rotenberg, A. Javadi, R. Schott, A. D. Wieck, A. Ludwig, M. C. Löbl, I. Söllner, R. J. Warburton, and P. Lodahl, "Quantum optics with near-lifetime-limited quantum-dot transitions in a nanophotonic waveguide," Nano Lett. **18**, 1801–1806 (2018).
28. R. Uppu, F. T. Pedersen, Y. Wang, C. T. Olesen, C. Papon, X. Zhou, L. Midolo, S. Scholz, A. D. Wieck, A. Ludwig, and P. Lodahl, "Scalable integrated single-photon source," Sci. Adv. **6**, eabc8268 (2020).
29. M. N. Makhonin, J. E. Dixon, R. J. Coles, B. Royall, I. J. Luxmoore, E. Clarke, M. Hugues, M. S. Skolnick, and A. M. Fox, "Waveguide coupled resonance fluorescence from on-chip quantum emitter," Nano Lett. **14**, 6997–7002 (2014).
30. G. Reithmaier, M. Kaniber, F. Flassig, S. Lichtmannecker, K. Müller, A. Andrejew, J. Vučković, R. Gross, and J. J. Finley, "On-chip generation, routing, and detection of resonance fluorescence," Nano Lett. **15**, 5208–5213 (2015).
31. P. Stepanov, A. Delga, X. Zang, J. Bleuse, E. Dupuy, E. Peinke, P. Lalanne, J.-M. Gérard, and J. Claudon, "Quantum dot spontaneous emission control in a ridge waveguide," Appl. Phys. Lett. **106**, 041112 (2015).
32. S. Kalliakos, Y. Brody, A. J. Bennett, D. J. P. Ellis, J. Skiba-Szymanska, I. Farrer, J. P. Griffiths, D. A. Ritchie, and A. J. Shields, "Enhanced indistinguishability of in-plane single photons by resonance fluorescence on an integrated quantum dot," Appl. Phys. Lett. **109**, 151112 (2016).
33. J. Liu, K. Konthasinghe, M. Davanço, J. Lawall, V. Anant, V. Verma, R. Mirin, S. W. Nam, J. D. Song, B. Ma, Z. S. Chen, H. Q. Ni, Z. C. Niu, and K. Srinivasan, "Single self-assembled InAs/GaAs quantum dots in photonic nanostructures: the role of nanofabrication," Phys. Rev. Appl. **9**, 064019 (2018).
34. C. L. Dreeßen, C. Ouellet-Plamondon, P. Tighineanu, X. Zhou, L. Midolo, A. S. Sørensen, and P. Lodahl, "Suppressing phonon decoherence of high performance single-photon sources in nanophotonic waveguides," Quantum Sci. Technol. **4**, 015003 (2018).
35. D. Najer, I. Söllner, P. Sekatski, V. Dolique, M. C. Löbl, D. Riedel, R. Schott, S. Starosielec, S. R. Valentin, A. D. Wieck, N. Sangouard, A. Ludwig, and R. J. Warburton, "A gated quantum dot strongly coupled to an optical microcavity," Nature **575**, 622–627 (2019).
36. M. Davanço, M. T. Rakher, D. Schuh, A. Badolato, and K. Srinivasan, "A circular dielectric grating for vertical extraction of single quantum dot emission," Appl. Phys. Lett. **99**, 041102 (2011).
37. L. Li, E. H. Chen, J. Zheng, S. L. Mouradian, F. Dolde, T. Schröder, S. Karaveli, M. L. Markham, D. J. Twitchen, and D. Englund, "Efficient photon collection from a nitrogen vacancy center in a circular Bullseye grating," Nano Lett. **15**, 1493–1497 (2015).
38. B. Yao, R. Su, Y. Wei, Z. Liu, T. Zhao, and J. Liu, "Design for hybrid circular Bragg gratings for a highly efficient quantum-dot single-photon source," J. Korean Phys. Soc. **73**, 1502–1505 (2018).
39. L. Rickert, T. Kupko, S. Rodt, S. Reitzenstein, and T. Heindel, "Optimized designs for telecom-wavelength quantum light sources based on hybrid circular Bragg gratings," Opt. Express **27**, 36824–36837 (2019).
40. S. Kolatschek, C. Nawrath, S. Bauer, J. Huang, J. Fischer, R. Sittig, M. Jetter, S. L. Portalupi, and P. Michler, "Bright Purcell enhanced single-photon source in the telecom O-band based on a quantum dot in a circular Bragg grating," Nano Lett. **21**, 7740–7745 (2021).
41. R. Harper, S. T. Flammia, and J. J. Wallman, "Efficient learning of quantum noise," Nat. Phys. **16**, 1184–1188 (2020).
42. S. Kako, C. Santori, K. Hoshino, S. Götzinger, Y. Yamamoto, and Y. Arakawa, "A gallium nitride single-photon source operating at 200 K," Nat. Mater. **5**, 887–892 (2006).
43. J. Liu, M. I. Davanço, L. Sapienza, K. Konthasinghe, J. V. de Miranda Cardoso, J. D. Song, A. Badolato, and K. Srinivasan, "Cryogenic photoluminescence imaging system for nanoscale positioning of single quantum emitters," Rev. Sci. Instrum. **88**, 023116 (2017).
44. C. Antón, J. C. Loredo, G. Coppola, H. Ollivier, N. Viggianiello, A. Harouri, N. Somaschi, A. Crespi, I. Sagnes, A. Lemaître, L. Lanco, R. Osellame, F. Sciarrino, and P. Senellart, "Interfacing scalable photonic platforms: solid-state based multi-photon interference in a reconfigurable glass chip," Optica **6**, 1471–1477 (2019).